

## Supplementary Materials

### **Plasmonic-driven charge separation through uniting Ag Nanoparticles (Ag NPs) form double Z-scheme heterostructure in WO<sub>3</sub>/BiOCl/g-C<sub>3</sub>N<sub>4</sub> for photocatalytic degradation antibiotics**

Zhangmeng Liu<sup>a\*</sup>, Shuaiqi Yao<sup>b</sup>, Yayao Li<sup>b</sup>

a School of Materials Science and Engineering, Hainan University, Haikou 570228, PR China

b School of Science, Hainan University, Haikou 570228, PR China

## 1. Materials

Bismuth nitrate pentahydrate ( $(\text{Bi}(\text{NO}_3)_3 \cdot 5\text{H}_2\text{O}, 99.0\%)$ ), sodium tungstate dihydrate ( $\text{Na}_2\text{WO}_4 \cdot 2\text{H}_2\text{O}, 99.5\%$ ) were obtained from Mclean Chemistry Co., Ltd., Polyvinylpyrrolidone K30 ( $(\text{C}_6\text{H}_9\text{NO})_n, \text{GR}$ ), Urea ( $\text{CH}_4\text{N}_2\text{O}, 99.0\%$ ), melamine ( $\text{C}_3\text{H}_6\text{N}_6, 99.0\%$ ) were purchased from Sinopharmaceutical Chemical Reagent Co., Ltd., hydrochloric acid (HCl), Sodium hydroxide (NaOH), ethanol absolute ( $\text{C}_2\text{H}_5\text{OH}$ , analytical reagent) was purchased from Xilong Science Co., Ltd., The scavenger reserve solution used to quench reactive substances is 10mM potassium iodide (KI) for trapping photo-generated holes ( $\text{h}^+$ ). 10mM isopropanol (IPA) is used to capture hydroxyl radical ( $\cdot\text{OH}$ ), 2 mM benzoquinone (BQ) for trapping superoxide radical ( $\cdot\text{O}_2^-$ ) in water, and 5-dimethyl-1-pyrrole-N-oxide (DMPO, 99.5%) were obtained from Mclean Chemistry Co., Ltd. All reagents are analytically pure and can be used without further treatment. Deionized water ( $18.2 \text{ M}\Omega \cdot \text{cm}$ ) was used for all preparations.

## 2. Characterization

The microstructure and morphology of the samples were observed by Talos F200X G2 (SEM) and (TEM). X-ray diffraction (XRD) patterns (Rigaku DX-2700BH), Fourier transforms infrared (FT-IR) spectroscopy (TENSOR 27, Bruker), and X-ray photoelectron spectroscopy (XPS) spectra were to characterize samples' crystal and molecular constitution. Optical performance was evaluated with a UV-Vis-NIR spectrophotometer ((Shimadzu, UV2450) and steady-state photoluminescence spectrum (PL, FLS 880). DMPO can be used to discover dynamic materials using electron spin resonance ((ESR) (MS 4000)).

## 3. Photocatalytic degradation procedure

Photocatalysis experiment uses a catalyst to degrade typical antibiotics (OFLX). The details are as follows: 20 mg catalyst with good dispersion and 50 mL antibiotic aqueous solution ( $20 \text{ mg L}^{-1}$ ) are contained in the quartz reaction tank. Firstly, the reaction tank is in a dark environment for 30 minutes to achieve the adsorption-desorption equilibrium. Then put, the reaction tank under a 300 W Xenon lamp to simulate the light of solar intensity. The reaction tank has a strict condensate system to maintain constant temperatures during photocatalytic reactions.

## 4. Preparation of WB-CN

A hydrothermal reaction prepared WB ( $\text{WO}_3/\text{BiOCl}$ ) heterojunction. In detail,  $\text{Bi}(\text{NO}_3)_3 \cdot 5\text{H}_2\text{O}$  (1.9425 g) was dissolved in HCl (20 mL 2 mol/L) to label as solution A,  $\text{Na}_2\text{WO}_4 \cdot 2\text{H}_2\text{O}$  (0.6612 g) and PVP (0.1025 g) were dissolved in 15 mL deionized water to label as solution B. Solution B was sonicated to obtain a fine dispersion and then slowly added to solution A under continuous stirring. Stirred the mixture for six hours to

make a homogeneous solution, which was then transferred into a polytetrafluoroethylene lining with a volume of 50 mL and placed in a stainless-steel autoclave, sealed, and placed in a drying box at 140 °C for 12 h. After cooling, the suspension in the reaction kettle was centrifuged to remove the supernatant, and the solid product was washed with deionized water and ethanol three times. The yellowish solid obtained by centrifugation was dried in a drying box at 60°C, and pure WB heterojunction was collected. Meanwhile, pure WO<sub>3</sub> was prepared under the same reaction conditions without the introduction of Bi (NO<sub>3</sub>)<sub>3</sub>•5H<sub>2</sub>O. Pure BiOCl was prepared under the same reaction conditions using Bi (NO<sub>3</sub>)<sub>3</sub>•5H<sub>2</sub>O and HCl as raw materials.

Based on a previous report with minor modifications [1]. The pure CN nanosheets were prepared by polymerizing the mixture of urea and melamine. A certain amount of urea and different mass of melamine (7.5-22.5%, every 5% as a gradient) were mixed by grinding, and the total group of urea and melamine was 7 g. The mixture was stored in a 50 mL crucible with a lid, put into a muffle furnace, and heated at a rate of 10 °C per minute to reach a final temperature of 550 °C. After three h, CN was obtained.

For the preparation of WB-CN heterojunction photocatalyst, a certain amount of CN and WB were all ultrasonically dispersed in 80 mL ethanol for four hours. They then stirred at room temperature for 12 h. The mixture was dried at 60 °C to collect the WB-CN photocatalyst. The obtained product was denoted as WB (2)-CN because the theoretical mass ratio of WB in the photocatalyst was 20%.

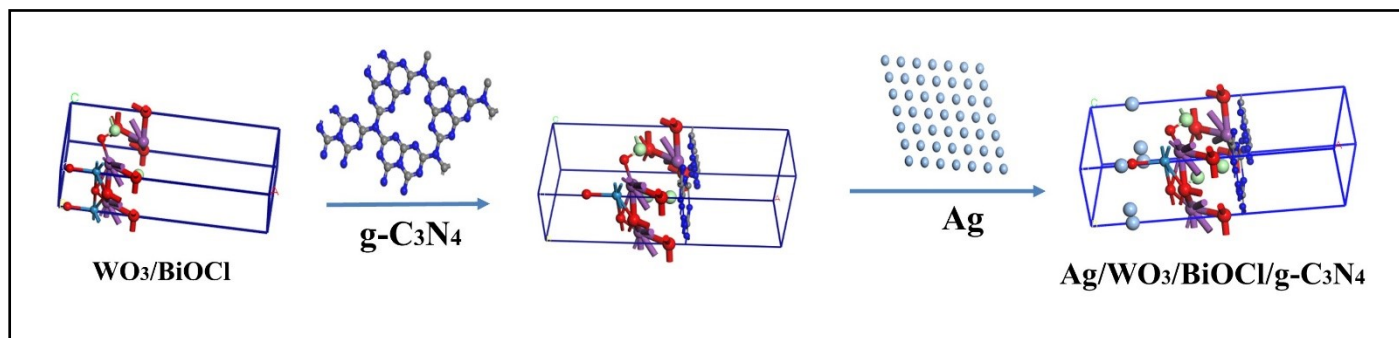
## 5. Photo-electrochemical measurements

Through CHI 760D electrochemical, the electrochemical impedance and photocurrent reaction of prepared photocatalysts were gauged in a conventional three-electrode system (CH Implements, Inc., China). The three electrodes consisted of catalyst-coated indium-doped tin oxide (ITO) glass (2 cm×2 cm) as the functional electrode, Pt wire as the counter electrode, and a strong calomel electrode (SCE) as the mentioned electrode. In the meantime, Na<sub>2</sub>SO<sub>4</sub> solution (0.1 M 50 mL) was utilized as an electrolyte solution. The functional electrode was prepared (500 μL) of the prepared dynamic substance on an ITO glass substrate through drop-casting an aliquot. An aliquot was prepared using dispersing the synthesized powdered sample's 1 mg ultrasonically with 5 mL of deionized water and the subsequent addition of 5 μL of Nafion solution (1%) as a binder. The temporary photocurrent (i-t) was deliberately consuming the equivalent 300W Xenon lamp at 0.5 V utilized potentiality. The electrochemical impedance spectroscopy (EIS) research was executed in the frequency scope of 1000 Hz -- 8000 Hz with a sinusoidal AC indication of 10 mV.

## 6. Theoretical calculation

States' density (DOS) and primordial cells' tape constitution were evaluated through the CASTEP

module. The generalized gradient estimation (GGA) of Perdew-Burke-Ernzerhof (PBE) operational is invoked for correlation and electron exchange. The level wave base's cutoff power is set to 450 eV, and the mutual space's k point is placed to an exceptional standard. The interaction between contiguous pictures in the optimization unit's computation is eradicated at the side of 15 vacuum layers. All the structures are completely relaxed, and the force tolerance is 0.02 eV. To optimize the geometric structure, the Monkhorst package point grid ( $36 \times 36 \times 25$  BiOCl,  $25 \times 25 \times 16$  WO<sub>3</sub>,  $9 \times 9 \times 3$  g-C<sub>3</sub>N<sub>4</sub>) was used to measure the Brillouin area.



Scheme 1. Simulated construction of Ag / WO<sub>3</sub> / BiOCl / g-C<sub>3</sub>N<sub>4</sub> atomic model

## 7. SEM and TEM images of samples

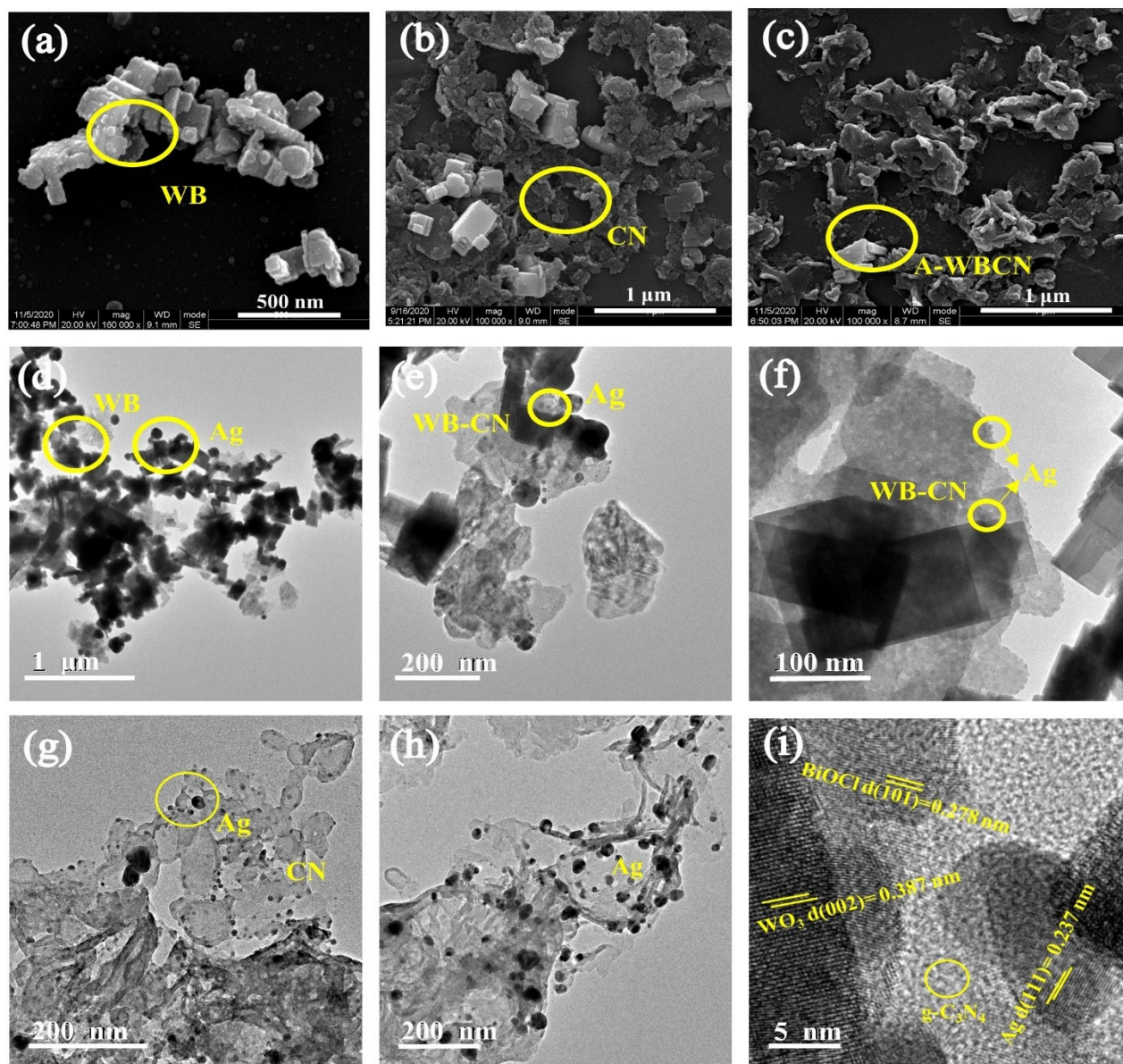


Fig.S1 SEM images of (a) A-WB, (b) WB-CN, (c) A-WBCN; TEM micrograph of (d) A-WB, (e) (f) A-WBCN, (g) (h) A-CN; (i) HRTEM image of A-WBCN

## 8. The XRD patterns of samples

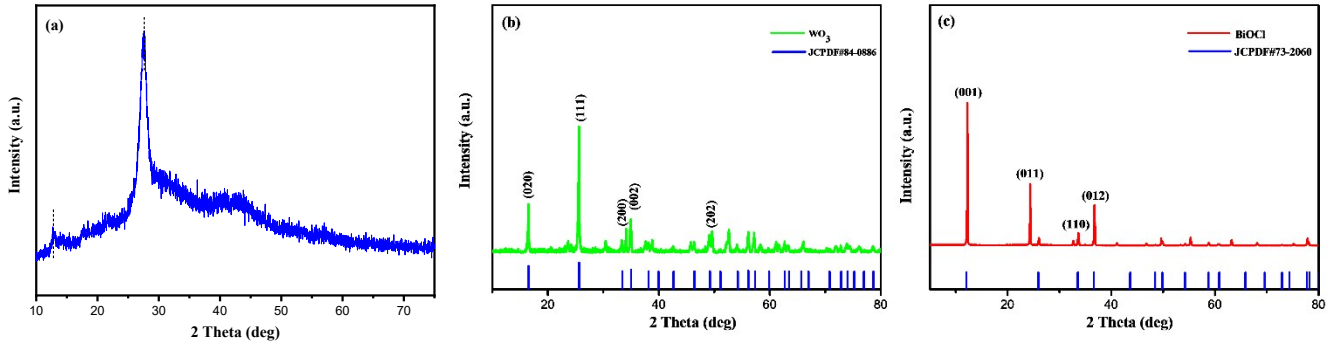


Fig. S2 XRD patterns of Pure (a) g-C<sub>3</sub>N<sub>4</sub>, (b) WO<sub>3</sub>, (c) BiOCl

## 9. EDX and XPS spectrum of A-WBCN

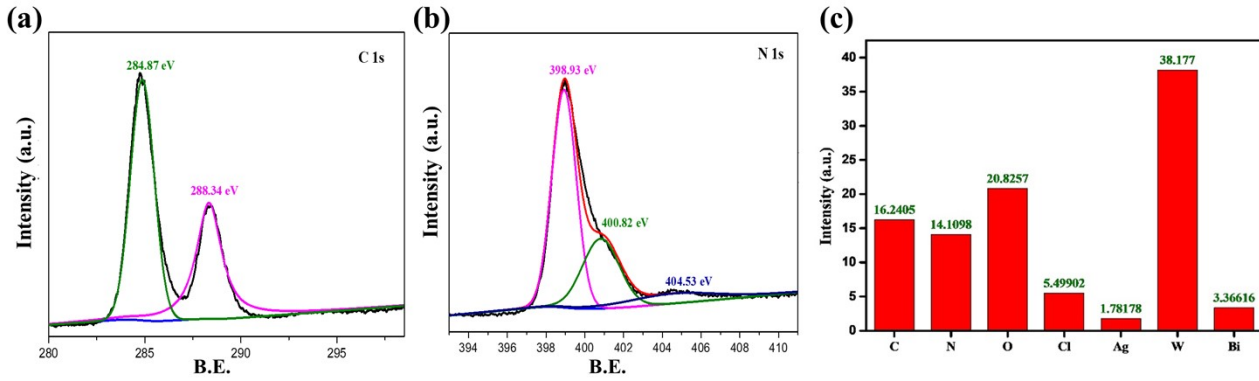


Fig. S3 (a) C 1s spectrum of A-WBCN; (b) N 1s spectrum of A-WBCN ; (c) EDX spectrum of A-WBCN

## 10. The VB- XPS spectra of CN, BiOCl, WO<sub>3</sub>

The bandgap was obtained by the following formula:

$$\alpha h\nu = A(h\nu - E_g)^{\frac{n}{2}} \quad (1)$$

Where  $\alpha$ ,  $h$ ,  $\nu$ ,  $A$ , and  $E_g$  was the optical absorption coefficient, Planck constant, optical frequency, constant, bandgap, respectively, and  $n$  was 0.5 for direct semiconductor WB and CN. Furthermore, according to Mullikan's theory, the  $E_{CB}$  and  $E_{VB}$  of photocatalyst could be obtained by the following equation:

$$E_{CB} = E_{VB} - E_g \quad (2)$$

$$E_{VB} = \chi - E^e + 0.5E_g \quad (3)$$

$E^e$ ,  $E_g$  was the geometric average of electronegativity of the composites, free-electron energy, and bandgap, respectively.

## 11. Effects of different ions in water and the initial pH value on the removal efficiency of OFLX

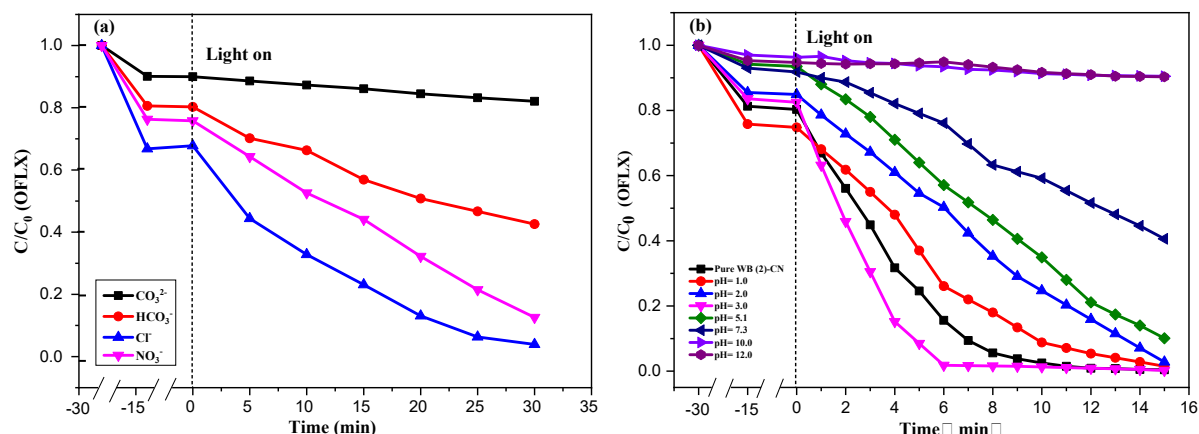


Fig. S4. (a) Different ions in water components on the photocatalytic degradation; (b) Effect of initial pH value on the removal efficiency of OFLX; Experiment conditions:  $[\text{OFLX}] = 100 \text{ mg/L}$ ;  $[\text{A-WBCN}] = 0.4 \text{ g/L}$

The natural water body is composed of a variety of chemical components, which may contain four common anions, such as  $\text{Cl}^-$ ,  $\text{HCO}_3^-$ ,  $\text{CO}_3^{2-}$  and  $\text{NO}_3^-$ . The effects of different anions on the degradation of OFLX by A-WBCN were investigated. The  $\text{Cl}^-$ ,  $\text{HCO}_3^-$ ,  $\text{CO}_3^{2-}$ ,  $\text{NO}_3^-$  salt solution with  $10 \text{ mmol} \cdot \text{L}^{-1}$  was mixed with OFLX solution, and the photocatalysis experiment was carried out. The experiment without adding ions was used as the blank control experimental group, and the results were shown in the Fig. S4(a). Anions can inhibit the photocatalytic degradation of OFLX by A-WBCN, and the order of inhibition is  $\text{CO}_3^{2-} > \text{HCO}_3^- > \text{NO}_3^- > \text{Cl}^-$ . In the dark reaction stage, anions can inhibit the adsorption of OFLX, and in the photo-reaction stage, the order of photocatalytic reaction rate is blank  $\text{Cl}^- > \text{NO}_3^- > \text{HCO}_3^- > \text{CO}_3^{2-}$ . These anions are free radical activity inhibitors, which will react with  $\cdot\text{O}_2^-$  and consume  $\cdot\text{O}_2^-$ , thus inhibiting the photocatalytic degradation of OFLX by A-WBCN. The addition of  $\text{CO}_3^{2-}$  and  $\text{HCO}_3^-$ , not only consumes  $\cdot\text{O}_2^-$ , but also changes the pH value of the solution, making the solution alkaline. The alkaline condition inhibits the photocatalytic degradation of OFLX by A-WBCN.  $\text{Cl}^-$  is adsorbed on the surface of the catalyst and occupies the active site, and  $\text{CO}_3^{2-}$  has two negative charges, which is stronger than  $\text{Cl}^-$  in consuming  $\cdot\text{O}_2^-$  free radicals, so the inhibitory effect is  $\text{CO}_3^{2-} > \text{HCO}_3^- > \text{NO}_3^- > \text{Cl}^-$ .

During the degradation reaction, the value of pH for the solution is one of the important factors affecting the photocatalytic rate. The surface charge and adsorption mode of catalysts and antibiotic pollutants will change with the change of pH value. In this experiment, the pH value of the degradation solution was

adjusted by HCl (1 mol·L<sup>-1</sup>) and NaOH (1 mol·L<sup>-1</sup>), respectively. The effects of A-WBCN adsorption and photocatalysis on the removal of OFLX were investigated under the conditions of pH=1.0, 2.0, 3.0, 5.1, 7.3, 10.0, 12.0, and the results are shown in the Fig. S4(b). With the increase of pH, the adsorption degradation rate and photocatalytic degradation rate of OFLX increased at first and then decreased, and the adsorption and photocatalytic degradation rate was the highest in pH=3.0. Under the condition of strong alkali, the photocatalytic degradation rate of OFLX decreased rapidly. It can be speculated that in a strong acid environment, WB is very unstable and easy to react to form H<sub>2</sub>WO<sub>4</sub> and Bi<sub>2</sub>O<sub>3</sub>, resulting in a great decrease in catalytic activity. In addition, the isoelectric point of WB is 6.29. When pH < 6.29, the surface of WB has a positive charge, and when pH value approaches 6.29, the positive charge decreases; when pH > 6.29, WB has a negative charge, and the negative charge increases with the increase of pH value. However, when the ionization constant of OFLX pK<sub>a</sub>=6.05, pH > 6.05, OFLX exists in molecular form, while when pH < 6.05, the active group in OFLX molecule begins to dissociate, the hydrogen bonding ability decreases, and OFLX changes from molecular state to surface negative charge, and the surface negative charge increases with the decrease of pH value. When pH value > 6.29, both OFLX and WB have negative charge on the surface, and with the increase of pH, the negative charge on the surface increases, and the mutual repulsive force between them increases, which leads to the weakening of adsorption effect and the decrease of photocatalytic efficiency. And the zero potential of CN is 2.1. Therefore, there is electrostatic attraction between the positive charge of CN and the negative charge of OFLX, which can accelerate the reaction during pH=3.0.

Under different pH conditions, the different surface charge of WB and OFLX leads to the difference of adsorption performance of A-WBCN to OFLX, which further affects the photocatalytic degradation ability of OFLX for A-WBCN. These results show that the synergistic effect between WB and CN is more beneficial to the degradation of OFLX under acidic conditions.

## 12. Modeling degradation kinetics

As reported in the literature [2], the degradation kinetics of most organic contaminants within a heterogeneous photocatalytic process fit the Langmuir-Hinshelwood (L-H) kinetic model.

$$r_0 = -\frac{dC_0}{dt} = \frac{K_{ads}k_{L-H}C_0}{1 + K_{ads}C_0} \quad (4)$$

$$t = \frac{1}{K_{ads}k_{L-H}} \ln \frac{C_0}{C} + \frac{1}{k_{L-H}}(C_0 - C) \quad (5)$$

$$\ln \frac{C_0}{C} = k_{app}t \quad (6)$$

where  $r_0$  is the initial rate of degradation ( $\text{mg L}^{-1} \text{min}^{-1}$ ), which is time-dependent,  $k_{L-H}$  is the constant rate of the reaction ( $\text{mg L}^{-1} \text{min}^{-1}$ ), and  $K_{ads}$  is the rate of OFLX adsorption on the surface of A-WBCN. The integrated form of (4) is given by (5). By ignoring the term  $(C_0-C)$  due to the low concentration of OFLX and assuming  $k_{app} = K_{ads} \cdot k_{L-H}$ , (Eq. 5) can be transformed into a pseudo-first-order kinetic model (6)

### 13. Comparison photodegradation efficiency of A-WBCN composite with other reported catalysts

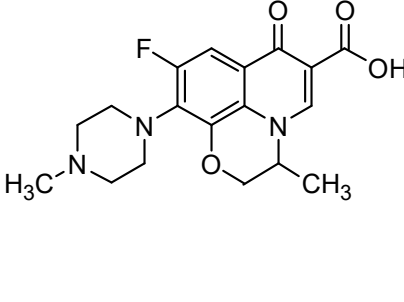
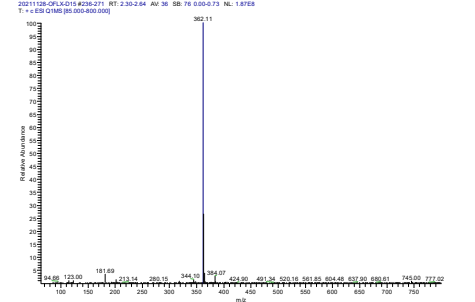
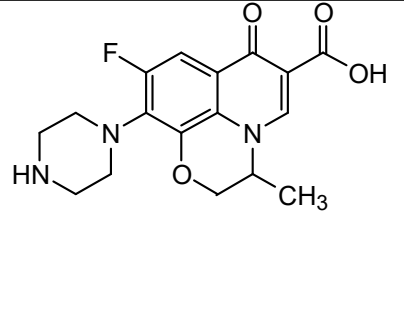
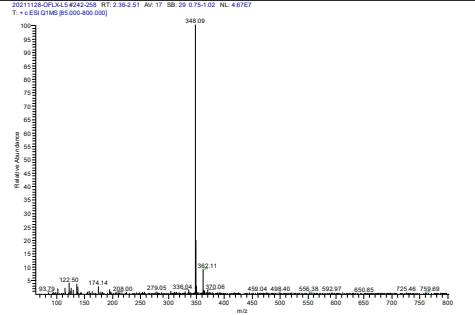
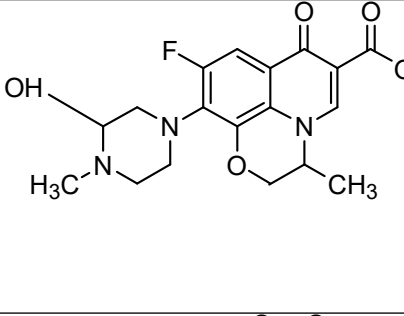
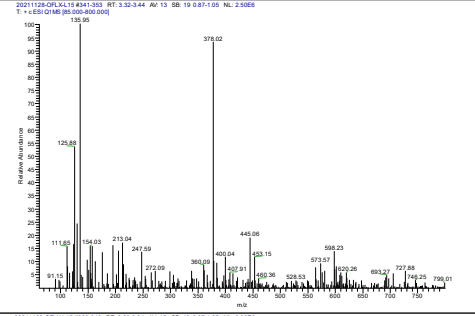
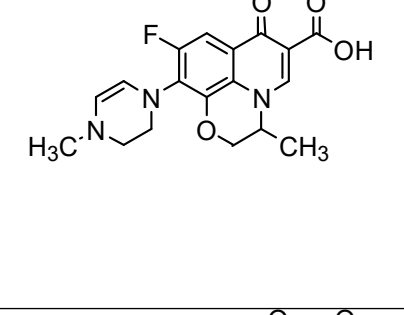
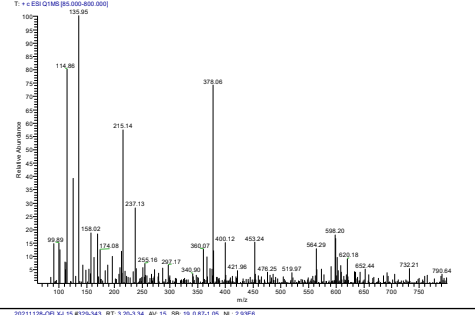
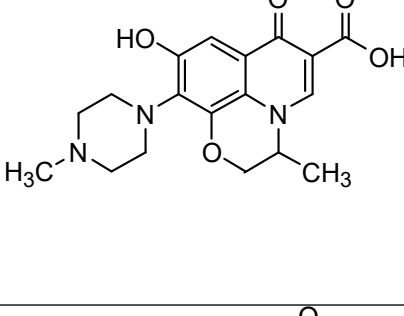
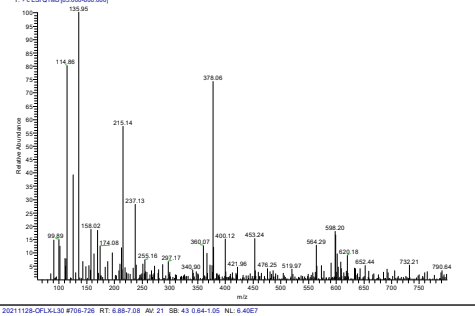
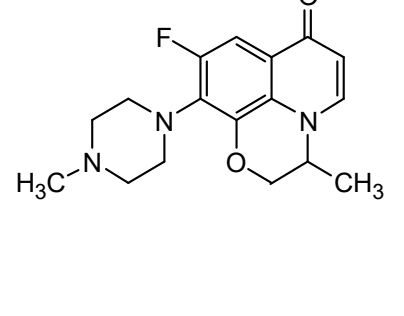
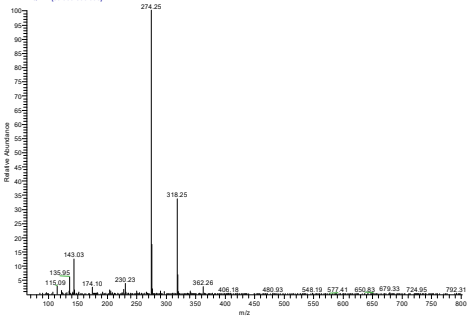
**Table.S1. A-WBCN and other types of photocatalysts towards OFLX degradation reported in the literature.**

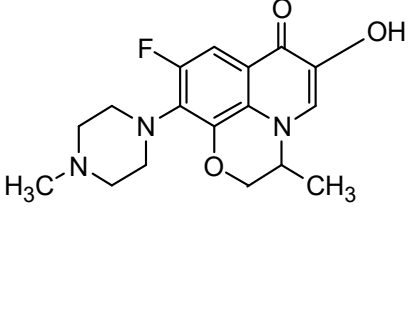
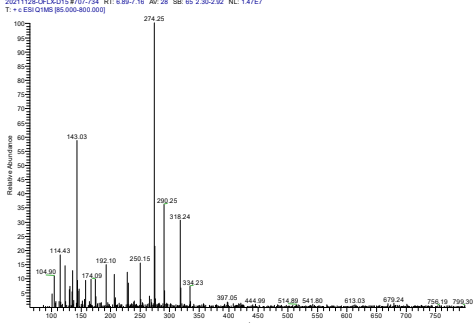
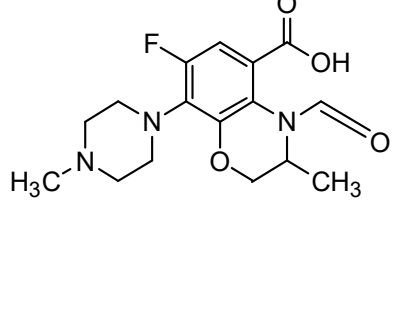
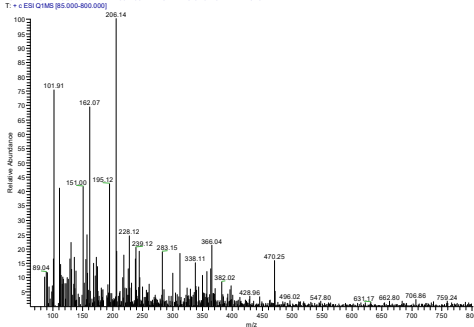
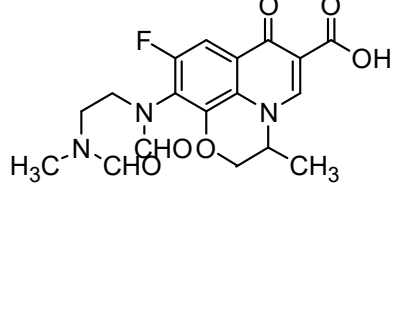
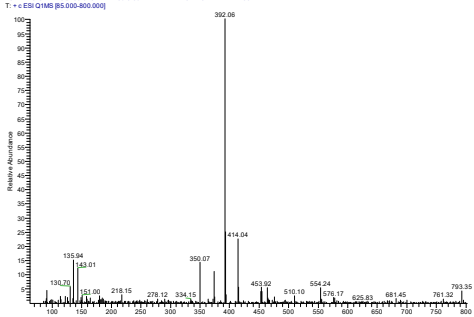
Photocatalyst	Catalyst	OFLX	Light source	Performance	Ref
$\text{Bi}_2\text{MoO}_6$	1g/L	10mg/L	Sunlight (55-65 Lux)	71% OFLX removal after 90 min	[3]
$\text{CdS}/\text{TiO}_2$	4.5g/L	10mg/L	85W Oreva bulb,4150 lumens	86% OFLX removal after 180 min	[4]
Bi/Ni co-doped $\text{TiO}_2$	1.5g/L	25mg/L	Seven 36W UV tubes(365nm)	86% OFLX removal after 360 min	[5]
Nanoparticles CdS	0.25g/L	10mg/L	85W Oreva CFL Bulb, 4150 lumens	86% OFLX removal after 360 min	[2]
Mpg- $\text{C}_3\text{N}_4/\text{CQDS}$	0.5g/L	10mg/L	Xe lamp (350 W),420 nm cut-off filter	90% OFLX removal after 120 min	[6]
MC/PDS	0.6 g/L	10 mg/L	Xe lamp (350 W), 420 nm cut-off filter	94.4% OFLX removal after 120 min	[7]
A-WBCN	0.4g/L	100 mg/L	Xe lamp (300 W)	90% OFLX removal after 20 min	This article

### 14. Time-dependent HPLC-MS spectra of TC and OFLX solution for WB-CN sample.

**Table. S2. The intermediates of OFLX by WB-CN under simulated light.**

Serial number	Structural	HPLC-MS data	m/z
---------------	------------	--------------	-----

<p>OFLX (1)</p>		 <p>2011128-OFLX10-#236-271 RT: 2.35264 Av: 38 SB: 76 600-73 NL: 18788 T: +ESI Q1MS (65.000-800.000)</p>	<p>362</p>
<p>(2)</p>		 <p>2011128-OFLX10-#242-258 RT: 2.36251 Av: 17 SB: 29 075-102 NL: 43787 T: +ESI Q1MS (65.000-800.000)</p>	<p>348</p>
<p>(3)</p>		 <p>2011128-OFLX10-#241-320 RT: 3.32-3.44 Av: 13 SB: 19 027-105 NL: 23058 T: +ESI Q1MS (65.000-800.000)</p>	<p>378</p>
<p>(4)</p>		 <p>2011128-OFLX10-#238-243 RT: 3.20-3.34 Av: 13 SB: 19 027-105 NL: 23058 T: +ESI Q1MS (65.000-800.000)</p>	<p>360</p>
<p>(5)</p>		 <p>2011128-OFLX10-#238-243 RT: 3.20-3.34 Av: 13 SB: 19 027-105 NL: 23058 T: +ESI Q1MS (65.000-800.000)</p>	<p>360</p>
<p>(6)</p>		 <p>2011128-OFLX10-#708-726 RT: 8.88708 Av: 21 SB: 43 024-100 NL: 64067 T: +ESI Q1MS (65.000-800.000)</p>	<p>318</p>

(7)			334
(8)			338
(9)			392

## 15. OFLX mineralization

The TOC removal efficiency was calculated by Eq. 7.

$$\text{TOC removal efficiency (\%)} = \frac{[\text{TOC}]_t - [\text{TOC}]_0}{[\text{TOC}]_t} \quad (7)$$

where  $[\text{TOC}]_0$  and  $[\text{TOC}]_t$  indicate the amount of total organic carbon at  $t = 0$  and  $t$ , respectively.

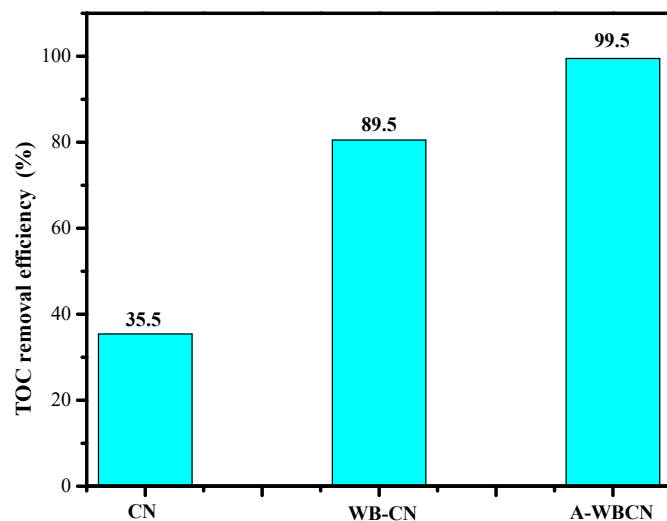


Fig.S5 TOC removal efficiency between A-WBCN and other photocatalyst materials

## 16. PDOS and Free radical capture experiments

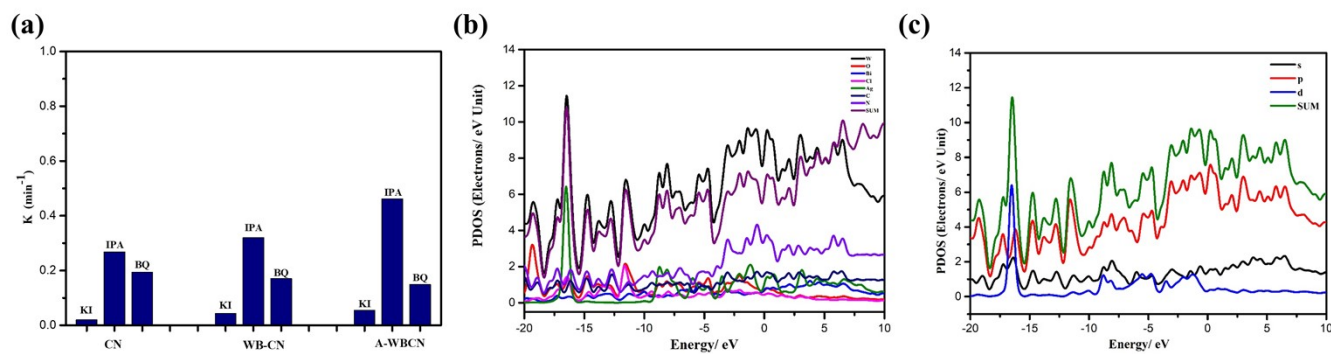


Fig. S6(a) Photo-degradation efficiency of OFLX by addition of scavenger; (b) estimated total density of states (TDOS) and (c) partial density of states (PDOS) for A-WBCN

## References

- [1] S. Chen, Y. Hu, X. Jiang, S. Meng, X. Fu, Fabrication and characterization of novel Z-scheme photocatalyst  $\text{WO}_3/\text{g-C}_3\text{N}_4$  with high efficient visible light photocatalytic activity, *Materials Chemistry and Physics*, 149-150 (2015) 512-521.
- [2] M. Kaur, S.K. Mehta, S.K. Kansal, Visible light driven photocatalytic degradation of ofloxacin and malachite green dye using cadmium sulphide nanoparticles, *Journal of environmental chemical engineering*, 6 (2018) 3631-3639.
- [3] G. Gupta, A. Umar, A. Kaur, S. Sood, A. Dhir, S. Kansal, Solar light driven photocatalytic degradation of Ofloxacin based on ultra-thin bismuth molybdenum oxide nanosheets, *Materials Research Bulletin*, 99 (2018) 359-366.
- [4] A. Kaur, A. Umar, W.A. Anderson, S.K. Kansal, Facile synthesis of  $\text{CdS}/\text{TiO}_2$  nanocomposite and their catalytic activity for ofloxacin degradation under visible illumination, *Journal of Photochemistry and Photobiology A: Chemistry*, 360 (2018) 34-43.
- [5] V. Bhatia, A.K. Ray, A. Dhir, Enhanced photocatalytic degradation of ofloxacin by co-doped titanium dioxide under solar irradiation, *Separation and Purification Technology*, 161 (2016) 1-7.
- [6] Y. Wang, F. Wang, Y. Feng, Z. Xie, Q. Zhang, X. Jin, H. Liu, Y. Liu, W. Lv, G. Liu, Facile synthesis of carbon quantum dots loaded with mesoporous  $\text{g-C}_3\text{N}_4$  for synergistic absorption and visible light photodegradation of fluoroquinolone antibiotics, *Dalton Transactions*, 47 (2018) 1284-1293.

- [7] D. Chen, Z. Xie, Y. Zeng, W. Lv, Q. Zhang, F. Wang, G. Liu, H. Liu, Accelerated photocatalytic degradation of quinolone antibiotics over Z-scheme MoO<sub>3</sub>/g-C<sub>3</sub>N<sub>4</sub> heterostructure by peroxydisulfate under visible light irradiation: Mechanism; kinetic; and products, Journal of the Taiwan Institute of Chemical Engineers, 104 (2019) 250-259.